Optoelectronic Characteristics of Nickel Cobaltite Nanoparticles-Decorated Porous Silicon Photodetector

Farah M. Wanas, Jasim K. Yasin*, Ohood J. Kadhum

Department of Physics, College of Science, University of Thi Qar, Nasiriyah, IRAQ
* Corresponding author email: jasimyaseen2019@gmail.com

Abstract
In this work, Nickel cobaltite ($NiCo_2O_4$) nanoparticles were incorporated into a porous silicon (PSi) structures prepared on silicon substrates by photoelectrochemical etching (PECE) technique. The electrical characteristics of the fabricated photodetector showed that the heterojunction of $NiCo_2O_4$ nanoparticles concentration of $4x10^{-4}$ M exhibits a relatively high photocurrent up to 2 mA. The optoelectronic characteristics showed a responsivity of 0.41 A/W, an external quantum efficiency of 0.78, and a detectivity of 6.57×10^{10} Jones. The response of the fabricated photodetector was evaluated via the ratio of response time to fall time, which was 0.82.

Keywords: Nickel cobaltite; Porous silicon; Heterostructures; Solution casting method
Received: March 2025; **Revised:** May 2026; **Accepted:** June 2026; **Published:** July 2026

1. Introduction

The hybrid heterojunction detectors are a qualitative revolution in optoelectronics and sensing techniques as they are based on the combination of the characteristics of inorganic and organic semiconductors at the nanoscale to create new functions not available in the individual components [1-3]. Semiconducting nanoparticles or quantum dots represent the fundamental component of the hybrid heterojunction detectors due to their unique optical and electronic characteristics governed by the quantum mechanics, mainly the quantum confinement effect, that allows controlling the energy bandgap and hence the absorption and emission wavelengths by controlling the particle size [4-7]. Such characteristics give these nanoparticles high sensitivity to light as well as high efficiency to generate electron-hole pairs when illuminated with radiation. However, the largest challenge is how to incorporate these nanoparticles in a functional structure allowing the collection of generated charges and transfer them efficiently to the electrodes [8-11]. Here, the role of porous silicon can be observed as an ideal platform for incorporation and hybridization.

The hybrid structures based on the incorporation of semiconducting ferrite or cobaltite nanoparticles – with unique optical and electrical characteristics – in porous silicon structures are reasonably promising for the applications of photodetectors and optoelectronic devices. These characteristics are originated from the synergetic effects resulted from the combination of the two nanoscale materials [12-16]. Optically, the porous silicon – as a porosity-controlled medium – participates to support light absorption via trapping and multi-directional scattering within the porous structure. This supports the ability of the ferrite or cobaltite nanoparticles to absorb light over a wide spectral range due to their semiconducting nature and relative narrow energy bandgap to extend the spectral responsivity of the photodetectors fabricated from these hybrid structures [17-20]. Furthermore, the possibility of enhanced magneto-optic effects to occur in such nanocomposites can induce some advanced applications to control light by magnetic fields [21-24].

In this work, nickel cobaltite nanomaterial was used to fabricate heterojunctions with a porous silicon layer formed on a silicon substrate formed by the photoelectrochemical etching (PECE) method. The optoelectronic properties of these heterojunctions were determined and analyzed.

2. Experimental Work

In order to prepare the porous silicon region on a p-type silicon substrate by the photoelectrochemical etching (PECE), as shown schematically, the silicon substrate was cut into 2.54x2.54 cm square samples. These samples were thoroughly cleaned with ethanol and distilled water, then kept in HF: ethanol (1:10) solution for 10 minutes. Then the sample was washed with deionized water and kept in methanol. It was placed inside the PECE cell, which contains (1:1) HF:ethanol solution for 10 minutes with 30 mA current and irradiated with a laser beam of 650 nm

wavelength. After completing the process, the sample was kept in methanol to prevent the oxidation and contamination from the surrounding environment.

A 10cm-diameter 99.9% purity $NiCo_2O_4$ target supplied by ALB Materials (USA) was sputtered to deposit $NiCo_2O_4$ thin films on glass substrates using DC plasma sputtering technique. The aqueous solutions of $NiCo_2O_4$ nanoparticles were prepared by dispersing specific weight (1 mg) of the $NiCo_2O_4$ nanoparticles in 10 mL of deionized distilled water to form a concentration of $4x10^{-4}$ M. The prepared solution was sonicated for 15 minutes and then 100 µL was taken and manually dropped on the porous silicon layer formed on the silicon substrate. The sample was left on the hotplate at 40°C for 30 seconds before dropping the next droplet. Aluminum contacts were deposited on the back side of the silicon substrate whereas silver paint was used to form the front electrode on the substrate's surface.

The optoelectronic characteristics of the fabricated heterojunctions were determined using a DC power supply and an accurate ammeter with a halogen lamp as a radiation source for illumination measurements.

3. Results and Discussion

Figure (1) shows the dark forward and reverse current-voltage characteristics of $CoFe_2O_4$ NPs-decorated PSi heterojunction measured in the voltage range of -4 to +4 V. The heterojunction exhibits rectifying properties as the forward current of this junction increases with bias voltage according to the diode equation. In the first region (low voltage region), the current increases slightly with voltage due to the recombination, while the second region shows that the current increases exponentially with bias voltage due to the domination of diffusion current over the recombination current. The reverse current increases slightly with reverse voltage for heterojunction. The ideality factor (n) of the heterojunction was determined using the following diode equation [25]:

$$I = I_0\left(e^{\frac{qV}{nk_BT}} - 1\right) \quad (1)$$

where I_0 is the saturation current, q is the electron charge, k_B is the Boltzmann coefficient, and T is the operating temperature. After using Eq. (1), the ideality factor for heterojunction prepared at $CoFe_2O_4$ concentrations of $4x10^{-4}$ M was 1.61. This value is within the typical range (1-2). The turn-on voltage of the prepared heterojunction, as shown in Fig. (1), was 1.8.

Figure (2) shows the spectral responsivity (R_λ) of $CoFe_2O_4$ NPs-decorated PSi heterojunction photodetectors fabricated using nanoparticles concentration of $4x10^{-4}$ M at two bias voltages of 5 and 10 V. The responsivity of the photodetector shows the maximum responsivity of 1.22 A/W at 650 nm and 5 V biasing voltage due to the absorption edge of $CoFe_2O_4$ film. The short wavelengths are absorbed in the film surface and the wavelengths are longer than the cut-off wavelength of $CoFe_2O_4$ film absorbed in PSi and Si substrate. The responsivity at the wavelength range of 500-700 nm comes from the light absorbed in PSi layer, while the wavelength longer than 700 nm is absorbed in the Si substrate. An increase in the bias voltage from 5 to 10 V results in an increase in the responsivity of the photodetector due to widening the depletion region and increasing the electric field. No effect of bias voltage on the position of the peak response was observed.

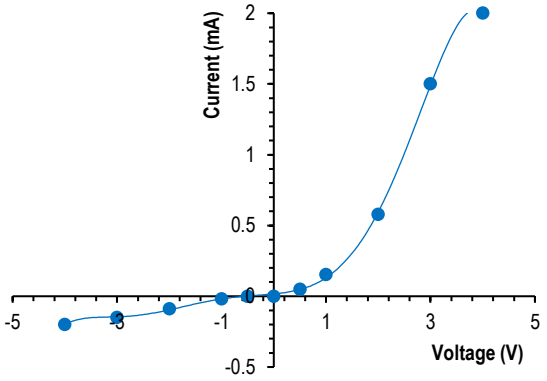

Fig. (1) I-V characteristics of the heterojunctions fabricated with $NiCo_2O_4$ NPs concentration of $4x10^{-4}$ M

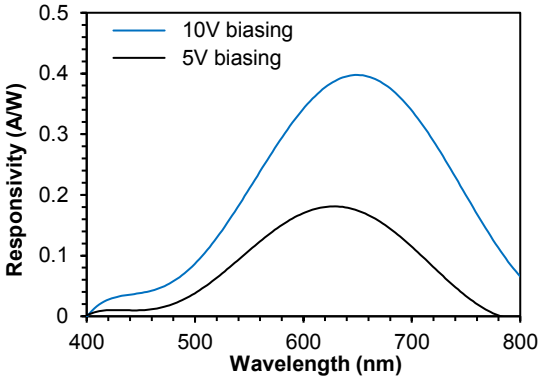

Fig. (2) Spectral responsivity plot of $NiCo_2O_4$ NPs-decorated PSi photodetectors fabricated with nanoparticles concentration of $4x10^{-4}$ M and at 5 V and 10 V biasing voltage

The external quantum efficiency EQE of the photodetector was calculated using the following relationship [259]:

$$EQE = \frac{1250\,R_\lambda}{\lambda\,(nm)} \quad (2)$$

Figure (3) shows the effect of bias voltage and $CoFe_2O_4$ layer thickness on the external quantum efficiency (EQE) of the photodetector. As shown, the maximum EQE value of 2.32% was achieved for the heterojunction at a wavelength of 650 nm and a biasing voltage of 5 V.

Figure (4) shows the specific detectivity (D^*) of the fabricated heterojunction photodetector at two different biasing voltages. The specific detectivity is

one of the important parameters of the photodetector, which describes the ability of the photodetector to detect the light signal. The specific detectivity can be estimated using the following equation [25]:

$$D^* = R_\lambda \sqrt{\frac{A}{2qI_{dark}}} \quad (3)$$

where I_d is the dark current at a certain bias voltage, and A represents the photosensitive area of the photodetector. The behavior of detectivity (D^*) is observed to follow a trend similar to that of spectral responsivity and external quantum efficiency. As the biasing voltage increases from 5 to 10 V, the detectivity (D^*) increases. This enhancement is attributed to the increased responsivity resulting from the widening of the depletion layer width at higher bias voltages, which improves carrier separation and reduces recombination losses. Consequently, more photo-generated carriers are collected, leading to higher detectivity.

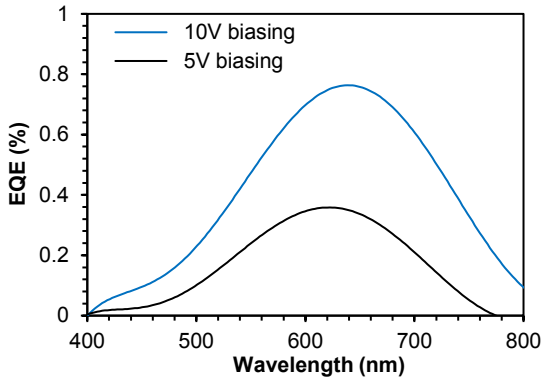

Fig. (3) Variation of the EQE of the heterojunctions fabricated with $NiCo_2O_4$ nanoparticles concentration of $4x10^{-4}$ M and biasing voltages of 5 V and 10 V

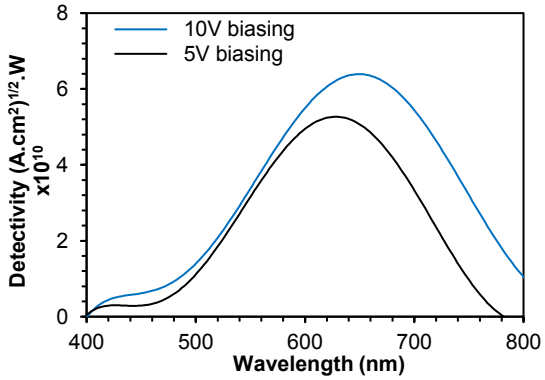

Fig. (4) Variation of specific detectivity (D^*) of fabricated heterojunction at biasing voltages of 5 V and 10 V

The noise equivalent power (NEP) of the photodetector was found to be dependent on the biasing voltage as shown in Fig. (5). A smaller NEP means that the photodetector has a better ability to detect weak signals.

The photodynamic response time is the most important parameter considered to determine how fast the photodetector response. Figure (6) shows the photodynamic response of the photodetector. The ratio of rise time to fall time for the fabricated photodetector was 0.82, at a bias voltage of -5 V. The reduced ration suggests that the photogenerated carriers experience more efficient transport and recombination due to the decreased absorption and enhanced carrier mobility in the $NiCo_2O_4$ layer [46]. The ON/OFF ratio (ON refers to illuminated state and OFF is the dark state) signifies the contrast between the photocurrent and dark current and was also determined.

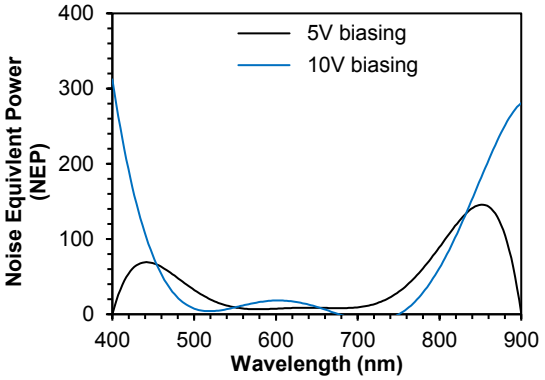

Fig. (5) Variation of NEP of fabrication heterojunction at biasing voltages of 5 V and 10 V

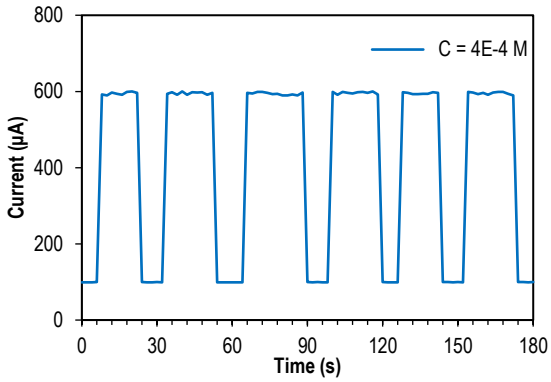

Fig. (6) Real-time photodynamic response of the fabricated photodetector (photocurrent response under on/off light illumination)

4. Conclusion

In conclusion, $NiCo_2O_4$NPs/PSi heterojunction photodetector was fabricated and characterized. The fabricated heterojunction exhibited rectifying behavior, with the I-V characteristics aligning with the recombination-tunneling model. The photodetector fabricated with a $NiCo_2O_4$ nanoparticles concentration of $4x10^{-4}$ M and biasing voltage of 5 V demonstrated superior photosensitivity compared to other devices fabricated with a larger thickness of this layer. The optimum photodetector showed a responsivity of 0.41 A/W, an external quantum efficiency (EQE) of 0.78, and a detectivity (D^*) of 6.57×10^{10} Jones.

References

[1] J.A.R. Ramón et al., "Inducing Superparamagnetism and High Magnetization in Nickel Cobaltite ($Ni_xCo_{3-x}O_4$) Spinel Nanoparticles by Controlling Ni Mole Fraction and Cation Distribution", *The J. Phys. Chem. C*, 124 (2020) 18264-18274.

[2] B. Sachin Kumar et al., "Graphene nanoclusters embedded nickel cobaltite nanofibers as multifunctional electrocatalyst for glucose sensing and water-splitting applications", *Ceram. Int.*, 45(18) (2019) 25078-25091.

[3] N. Cárdenas et al., "Synthesis and characterization of nickel cobaltite–supported film for hexavalent chromium photocatalytic reduction", *Water Sci. Technol.*, 90(7) (2024) 2131-2145.

[4] A. Fatoni et al., "Glucose biosensor based on activated carbon – $NiFe_2O_4$ nanoparticles composite modified carbon paste electrode", *Result Chem.*, 4 (2022) 100433.

[5] S.S. Vadla et al., "Electrodeposited $NiFe_2O_4/Cu_2O$ heterostructure thin films with enhanced photocurrent generation", *J. Photochem. Photobiol.*, 15 (2023) 100181.

[6] A.R. Malik et al., "Lime peel extract induced $NiFe_2O_4$ NPs: Synthesis to applications and oxidative stress mechanism for anticancer, antibiotic activity", *J. Saudi Chem. Soc.*, 26(2) (2022) 101422.

[7] S. tul Shafa et al., "Synthesis and characterization of Cu and Tb substituted $NiFe_2O_4$@MXene nanocomposite as a new photocatalyst for removal of organic dyes and drugs from industrial wastewater", *Result Phys.*, 63 (2024) 107844.

[8] R. Devi et al., "Au/$NiFe_2O_4$ nanoparticle-decorated graphene oxide nanosheets for electrochemical immunosensing of amyloid beta peptide", *Nanoscale Adv.*, 2(1) (2020) 239-248.

[9] B. Godbole et al., "Synthesis, Structural, Electrical and Magnetic Studies of Ni- Ferrite Nanoparticles", *Phys. Procedia*, 49 (2013) 58-66.

[10] F.J. Kadem, B.T. Chead and U.A. Yaseen, "Characteristics of Nickel Ferrite Nanostructures Prepared by DC Reactive Magnetron Co-Sputtering", *Iraqi J. Sci. Indust. Res.*, 3(4) (2024) 19-22.

[11] F.J. Kadhim and R.A. Mohammed, "Structural Characteristics of Nickel Ferrite Nanoparticles Synthesized by New Arrangement of Concentric Targets in DC Reactive Magnetron Sputtering", *Iraqi J. Appl. Phys.*, 12(4) (2016) 9-12.

[12] J. Haman, "New Geometrical Arrangement to Prepare Nickel Ferrite Nanostructures on Glass Substrates Using DC Reactive Magnetron Sputtering", *Iraqi J. Sci. Indust. Res.*,, 3(2) (2024) 42-46.

[13] R. Kurosawa et al., "Variations in the saturation magnetization of nanosized $NiFe_2O_4$ particles on adsorption of carboxylic acids", *J. Asian Ceram. Soc.*, 2(1) (2014) 41-43.

[14] J.L. Domínguez-Arvizu et al., "Study of $NiFe_2O_4/Cu_2O$ p-n heterojunctions for hydrogen production by photocatalytic water splitting with visible light", *J. Mater. Res. Technol.*, 21 (2022) 4184-4199.

[15] S. Kamal et al., "Synthesis of boron doped $C_3N_4/NiFe_2O_4$ nanocomposite: An enhanced visible light photocatalyst for the degradation of methylene blue", *Result. Phys.*, 12 (2019) 1238-1244.

[16] E. Pérez, G. Marquez and V. Sagredo, "Effect of Calcination on Characteristics of Nickel Ferrite Nanoparticles Synthesized by Sol-Gel Method", *Iraqi J. Appl. Phys.*, 15(1) (2019) 13-17.

[17] H. Wang et al., "One-pot solvothermal preparation of MFe_2O_4 (M=Ca, Mg and Ni) ferrite- graphene oxide nanocomposites for adsorption of acridine orange", *Desalin. Water Treat.*, 298 (2023) 174-183.

[18] A.J. Raheem and S.M. Raji, "Nickel Ferrite Nanostructures Prepared by DC Reactive Magnetron Sputtering", *Iraqi J. Appl. Phys. Lett.*, 7(2) (2024) 7-10.

[19] R. Tiwari et al., "Structural and magnetic properties of tailored $NiFe_2O_4$ nanostructures synthesized using auto-combustion method", *Result Phys.*, 16 (2020) 102916.

[20] T. Shanmugavel et al., "Tailoring the Structural and Magnetic Properties and of Nickel Ferrite by Auto Combustion Method", *Procedia Mater. Sci.*, 6 (2014) 1725-1730.

[21] M.A. Shilpa Amulya et al., "Sonochemical synthesis of $NiFe_2O_4$ nanoparticles: Characterization and their photocatalytic and electrochemical applications", *Appl. Surf. Sci. Adv.*, 1 (2020) 100023.

[22] A. Safdar et al., "Biogenic synthesis of nickel cobaltite nanoparticles via a green route for enhancing the photocatalytic and electrochemical performances", *Sci. Rep.*, 14 (2024) 17620.

[23] M.A. Abduljabar and S.H. Merza, "Synthesis, Characterization of Nickel Cobaltite Nanoparticles and Its Use in Removal Methyl Green Dye from Aqueous Solution", *Ibn Al-Haitham J. Pure Appl. Sci.*, 37(3) (2024) 264-278.

[24] O.A. Hammadi and N.E. Naji, "Characterization of polycrystalline nickel cobaltite nanostructures prepared by DC plasma magnetron co-sputtering for gas sensing applications", *Phot. Sens.*, 8 (2018) 43-47.

[25] S.M. Sze and K.K. Ng, **"Physics of Semiconductor Devices"**, 3rd ed., Wiley-Interscience (NJ, 2007), p. 119, 618, 667, 125, 666.

